JOURNAL OF GEOPHYSICAL RESEARCH, VOL. 101, NO. D21, PAGES 26,527–26,538, NOVEMBER 27, 1996

Hydrologic applications of satellite data: 2. Flow simulation and soil water estimates

Alexandre K. Guetter and Konstantine P. Georgakakos[1]
Hydrologic Research Center, San Diego, California

Anastasios A. Tsonis
Department of Geosciences, University of Wisconsin, Milwaukee

Abstract. The uncertainty in streamflow simulations and soil water estimates associated with satellite rainfall forcing is investigated for the Upper Des Moines River basin in the midwestern United States. Synthetic series of satellite rainfall estimates were produced with a rain gauge-satellite stochastic model and 10 years of daily rain gauge data (1979-1988) for three basins with drainage areas ranging from 2,000 km^2 to 14,000 km^2. The synthetic satellite rainfall series was based on observed satellite visible and infrared data which provided estimates of satellite rainfall for 180 randomly selected days in the period 1980-1987. Streamflow and soil water estimates were obtained with a rainfall-runoff-routing model (3R), based on soil water balance and accounting for snowmelt and frozen ground effects. Sensitivity of flow prediction with respect to rainfall was examined for three different conditions: (1) 3R calibrated and forced with rain gauge data, (2) 3R calibrated with rain gauge data and forced with satellite rainfall, and (3) 3R calibrated and forced with satellite rainfall. The most important results regarding the effect of satellite rainfall on flow simulation and soil water estimation for climate studies are as follows: (1) Flow simulation accuracy is sensitive to the basin scale, yielding higher correlation of simulated with observed streamflow for larger scales, (2) the hydrologic model forced with satellite data possesses skill during the period May–July for the midwestern United States, (3) derived upper soil water estimates are similar to the ones obtained using rain gauge forcing, and derived lower soil water estimates are lower than those obtained from rain gauge forcing.

1. Introduction

Several techniques and algorithms have been developed to estimate rainfall from satellite data (e.g., *Engman* [1993] for a broad review; *Wilheit et al.* [1994], for rainfall from passive microwave measurements; and *Adler et al.* [1994] for adjusting infrared rainfall estimates with microwave measurements). In part 1 of this study [*Tsonis et al.*, this issue] daily mean-areal rainfall estimates were obtained for a number of days over a 208 x 336 km^2 area in the midwestern region of the United States, using (GOES) visible and infrared temperature data. The large spatial coverage of satellite data makes it attractive for climatological studies [*Negri et al.*, 1994; *Adler et al.*, 1994], and it is expected that use of satellite rainfall products will be the main source of hydrological information for several regions of the globe. However, several questions remain to be answered about the implication of using satellite rainfall to estimate hydrologic states and fluxes. This paper characterizes the errors in streamflow and soil water estimates of a hydrologic model forced by satellite rainfall on two different scales (3,000 km^2 and 14,000 km^2).

The goals of the analysis are (1) to assess the adequacy of satellite rainfall for flow simulation over large catchments, (2) to estimate the errors in streamflow and soil water estimates expected when using satellite rainfall for climate studies, (3) to estimate the uncertainty in flow simulation when satellite rainfall is given as input to hydrologic-hydraulic models calibrated with extended series of daily rain gauge data. It is noted that the first goal is relevant also to long-term prediction using conditional Monte Carlo simulation, such as used in the National Weather Service (NWS) extended streamflow prediction (ESP) components [e.g., *Georgakakos et al.*, 1995a; *Day*, 1985].

Streamflow and soil water estimates were obtained with a physically based, conceptual, rainfall-runoff-routing (3R) model. The 3R model is a simplified version of the operational hydrologic forecast component of the operational NWS River Forecast System. It accounts for two zones of soil water (soil water is the equivalent depth of liquid water in the top ~2-m layer of soil), snow accumulation and ablation, frozen ground effects, and channel routing. The model requires mean-areal precipitation and evapotranspiration as input and concurrent series of streamflow for parameter calibration and validation. The 3R calibration procedure is designed to conserve mass (long-term average predicted streamflow should be equal to observed streamflow), and to mimic daily flow variability. The cross correlation between daily predicted and observed streamflow exceeded 0.88 for 3R calibrated with rain gauge data, and varied in the range 0.77-0.85 for calibration with satellite rainfall, with negligible bias in both cases.

This study assumes that the network of 29 rain gauges in the Upper Des Moines River basin provides the ground-truth for mean-areal precipitation estimates over areas greater than 2,000 km^2 [*Bae and Georgakakos*, 1992]. Our methodology

[1] Also at Scripps Institution of Oceanography, University of California at San Diego, La Jolla, California

Copyright 1996 by the American Geophysical Union.

Paper number 96JD01655.
0148-0227/96/96JD-01655$09.00

consists of (1) simulating a 10-year series of daily satellite mean-areal rainfall for three basins of different sizes and latitudes, (2) calibrating the 3R model with local rain gauge and large-scale satellite data, (3) computing streamflow errors and soil water discrepancies associated with the use of satellite rainfall, and for 3R calibrated independently, first with rain gauge and then with satellite data.

The next section presents a brief description of the study catchments. Section 3 summarizes the sampled satellite rainfall information and the resulting 10-year series of synthetic satellite rainfall estimates. It is followed by the 3R model description, parameter estimation, and effects of using satellite data on parameter estimates, in section 4. Streamflow simulation uncertainty, sensitivity of soil water estimates, and sensitivity of soil water spatiotemporal scaling are presented in sections 5 and 6, respectively. Section 7 contains conclusions and recommendations.

2. Basin Description

The Upper Des Moines River basin is located in Minnesota and northcentral Iowa (42-44°N and 94-96°W). The drainage area is about 14,000 km^2 of gently rolling terrain, mainly cultivated with corn and soybean fields. This area is typical of midcontinental hydrologic regimes in the United States and has midcontinental extratropical climate. The physiographic and hydrologic characteristics of the Upper Des Moines River basin were described by *Bae and Georgakakos* [1994], *Georgakakos and Bae* [1994], and *Georgakakos et al.* [1995a,b]. In this study, satellite rainfall estimates and streamflow predictions are computed for two headwater subbasins, namely the West Fork Des Moines River with outlet at Estherville, Iowa, and the Boone River with outlet at Webster City, Iowa, and for the larger Upper Des Moines River basin with outlet at Stratford, Iowa.

The West Fork Des Moines River at Estherville, called West Fork hereinafter, is located on the northwest corner of the Upper Des Moines River basin, and it drains an area of 3,500 km^2. West Fork is characterized by a large number of lakes and extended periods with frozen ground which affects the dynamics of soil water response to precipitation (snowfall) in winter and early spring. The Boone River at Webster, called Boone hereinafter, drains 2,200 km^2, and is located on the southeast corner of the Upper Des Moines River basin. The latitudinal separation between West Fork and Des Moines is about 1.5°. The Upper Des Moines River basin at Stradford, called Des Moines hereinafter, includes the West Fork, Boone and four other subbasins [see *Bae and Georgakakos*, 1992, for details] draining 14,000 km^2.

The climatological annual total precipitation and streamflow over the Upper Des Moines are 770 mm yr^{-1} and 150 mm yr^{-1}, with major floods resulting from heavy rainfall during the summer months or from snowmelt, often accompanying rain, in late winter and early spring. Maximum monthly rainfall is in June, while maximum rainfall variability is in September. The three basins are characterized by a bimodal streamflow climatology. *Georgakakos et al.* [1995a] has shown that the streamflow climatology for the Boone River peaks in midspring and midsummer. The midspring streamflow peak is associated with the concurrent saturation of the upper layers of soil, following a winter and early spring period of reduced percolation due to frozen ground [Figure II-2.5, *Georgakakos et al.*, 1995a]. The midsummer streamflow peak is associated with high soil moisture in both the upper and lower layers and with heavy precipitation. The two modes of the bimodal streamflow climatology for both West Fork and Des Moines are less pronounced than in Boone, with the midspring streamflow peak dominating the streamflow annual cycle. *Cayan and Georgakakos* [1995] show that the spatial scale of precipitation that is responsible for seasonal soil water anomalies in Boone is much larger than the basin area.

3. Satellite Rainfall

Tsonis et al. [this issue] described the mean-areal satellite rainfall estimates for a 70,000-km^2 area that includes the Des Moines basin, using a random sample of 180 days from the period May-September in 1982-1988. In lieu of a long continuous record of satellite rainfall estimates over the area of interest we extended the series of satellite rainfall for climate studies. At first, we investigated the linear relationship and error structure of concurrent mean-areal satellite rainfall and rain gauge measurements, and then constructed extended series of satellite rainfall estimates based on surrogate daily rain gauge data. We applied the National Weather Service method of inverse-distance weighted average for the computation of daily mean-areal precipitation from daily rain gauge observations [*Larson and VanDemark*, 1979] over West Fork, Boone and Des Moines. *Georgakakos et al.* [1995b] show that the cooperative observer rain gauge network in the area is adequate for the computation of mean-areal rainfall estimates over areas of order 2,000 km^2 and greater. The sample of 51 rainy days yielded cross correlations of rain gauge and satellite rainfall that varied from 0.79 (Boone and Des Moines) to 0.46 (West Fork). However, more than half of the cases corresponded to mean-areal rain gauge estimates smaller than 2.5 mm day^{-1} for which a wide range of satellite estimates was found. This wide range of estimates was due to two tendencies of the satellite rainfall estimation procedure: (a) underestimation of the number of days with rainfall, and (b) overestimation of the amount of rainfall when significant rainfall was in the area. It is noted that small mean-areal rainfall intensities obtained from a rain gauge network are often related to small-scale precipitation events associated with or without extensive high clouds.

A synthetic series of satellite rainfall was built for each of the three basins based on multidecadal daily series of mean-areal rain gauge observations and a model contingent on a threshold, P_τ. P_τ is the maximum intensity of rain gauge mean-areal precipitation for which the satellite-based estimates show zero rain with a large probability. The algorithm follows a Bernoulli distribution, $B(1,p)$, for $0 \le P_r \le P_\tau$, in which P_r is rain gauge mean-areal precipitation and p is the probability that satellite rainfall is $P_s=0$ when the rain gauge mean-areal rainfall is less than P_τ. The probability that $P_s \ne 0$ is $(1-p)$ for $P_r \le P_\tau$, and the sampled satellite data shows that the corresponding P_s can be as high as 10 mm d^{-1}. When $0 \le P_r \le P_\tau$, a random number (r_n) is generated; if $r_n \le p$, then $P_s=0$, otherwise P_s is obtained from a uniform distribution $U(0,10)$. Equation (1) describes the algorithm for $P_r > P_\tau$,

$$P_s = a_s(P_r) + b_s + e_s \qquad (1)$$

in which α_s and β_s are the regression coefficients between the satellite and rain gauge rainfall, and ε_s is the Gaussian deviate of the sampled satellite and modeled rainfall residuals. The

Table 1. Parameters of the Synthetic Satellite Rainfall Algorithm

Basin	p	P_τ, mm d^{-1}	μ, mm d^{-1}	α	β	$\sigma_{residual}$
Boone	0.77	2.5	8.14	0.514	1.14	3.3
West Fork	0.75	2.5	6.85	NS*	NS*	4.9
Des Moines	0.79	2.5	8.48	0.261	5.64	4.3

NS* is not significant at the 90% confidence level.

regression coefficients α_s and β_s exceeded the 90% significance level for Boone and Des Moines, whereas the linear relation between rain gauge and satellite rainfall was not significant at the 90% confidence level for the West Fork; in this latter case the algorithm was modified to $P_s=\mu+\varepsilon_s$, in which μ is the mean of the satellite rainfall sample and ε_s is a Gaussian deviate. Table 1 summarizes the parameters of the synthetic satellite rainfall algorithm for the three basins.

Synthetic daily satellite rainfall for the period May-September was computed from 1965 to 1988 for the three basins. The satellite procedure underpredicted rainfall volumes, variability and number of rainy days, as indicated in Table 2 and Figure 1. It produced higher rainfall rates, but for fewer rainy days. The large number of rain gauge rainy days is an artifact of the spatial averaging procedure which distributes small-scale local rainfall values over a large area. Figures 1a and 1b indicate that satellite rainfall climatology (thick solid line) and interannual variability (thick dotted line) are underpredicted for Boone and West Fork, whereas Figure 1c shows that satellite rainfall matches rain gauge climatology for the 14,000 km^2 Des Moines basin. In the latter case, satellite rainfall interannual variability is also underpredicted.

Two factors affect the synthetic series bias: (1) the threshold P_τ by assigning no-rain satellite observation to either light or spotty rainfall ($0<P_r<2.5$ mm d^{-1}), and (2) the parameters of the regression model, by underestimating heavy rainfall ($P_r>15$ mm d^{-1}). The sensitivity of the synthetic series bias to P_τ is shown in Table 3, which lists the ratio of satellite and rain gauge rainfall for $0\le P_\tau\le 2.5$ mm d^{-1} for the three basins. There is a small variation of the bias with respect to P_τ for Boone (small regression constant), whereas the variation is significant for West Fork and Des Moines (large regression constant). The threshold $P_\tau=2.5$ mm d^{-1}, obtained by sample inspection is used in the remainder of the analysis. It is conjectured that the bias found is characteristic of the satellite rainfall estimation procedure when large-area estimates are used for small areas (<3,500 km^2).

4. Hydrologic Model

For this work, an adaptation of the operational National Weather Service model was utilized with a hydraulic routing model (3R) for flow simulation and soil water estimation in the three midwestern catchments. The soil moisture accounting component of the rainfall-runoff model used in the tests is the modified Sacramento model, documented by *Bae and Georgakakos* [1994]. It is a conceptual spatially lumped model suitable for application to headwater drainage basins. It accepts mean-areal precipitation and mean-areal evapotranspiration as input, and produces total channel inflow as output. The flow components that contribute to the total channel inflow are surface runoff in cases of excessive rainfall rates, interflow through the upper soil layers, and groundwater flow. The model subdivides the drainage basin into two zones: an upper zone and a lower zone. The upper zone simulates water stored in the upper soil layers which is available for evapotranspiration, percolation, surface runoff, and interflow. The lower zone simulates groundwater storage.

Snowmelt is an important source of channel flow for many midwestern catchments in early spring. Moreover, frozen ground effects on interflow and percolation are important during winter. Reduced percolation rates due to frozen ground play an important role on the lower soil state and on the interseasonal memory of the system. We used the lumped, conceptual, temperature-index, snow model developed by *Anderson* [1973] to simulate snow accumulation, ablation and frozen ground effects. This model is currently used by the U.S. National Weather Service for operational flow forecasting, and was recently applied for climate studies of the Upper Des Moines River basin by *Bae and Georgakakos* [1992].

The 3R differs from the Sacramento model by allowing for just one soil compartment in each of the soil zones and no distinction is made between free and tension-bound soil water [e.g., *Peck*, 1976; *Bae and Georgakakos*, 1994]. The 3R does use the same nonlinear percolation function to transfer water from the upper to the lower zone. The governing equations of the soil moisture accounting model and corresponding fluxes (in millimeters per day) are given below, where dependence of states and fluxes on time is implicit.

$$\frac{dX_1}{dt} = P - SR - PC - ET_1 - INT \tag{2}$$

$$\frac{dX_2}{dt} = PC - ET_2 - GW \tag{3}$$

$$SR = P\left(\frac{X_1}{X_1^0}\right)^{m_1} \tag{4}$$

Table 2. Statistics of Rain Gauge and Synthetic Satellite Rainfall for May-September of 1965-1988

Basin	Average Rain Gauge, mm d^{-1}	Average Satellite mm d^{-1}	Standard Deviation Rain Gauge, mm d^{-1}	Standard Deviation Satellite, mm d^{-1}	Satellite and Rain Gauge Cross Correlation	Number of Rainy Days-Rain Gauge, days mo^{-1}	Number of Rainy Days-Satellite, days mo^{-1}
Boone	3.46	2.39	7.61	4.53	0.87	18.0	9.8
West Fork	2.94	2.25	6.26	4.02	0.49	16.6	9.2
Des Moines	3.11	2.99	5.76	4.58	0.67	21.0	11.2

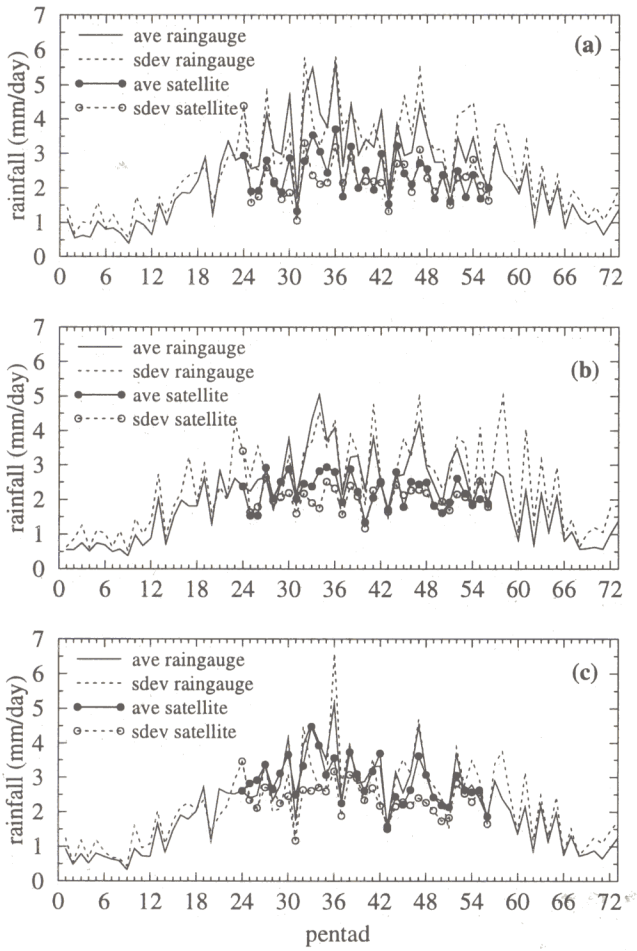

Figure 1. Rain gauge and satellite rainfall pentad climatologies (1965-1988) for (a) Boone, (b) West Fork and (c) Des Moines. The lines with symbols correspond to satellite rainfall average and standard deviation for May-September (pentads 24-56).

$$ET_1 = PET\left(\frac{X_1}{X_1^0}\right) \tag{5}$$

$$PC = C_{FRG}C_2X_2^0\left[1 + C_3\left(1 - \frac{X_2}{X_2^0}\right)^{m2}\right]\left(\frac{X_1}{X_1^0}\right) \tag{6}$$

$$INT = C_{FRG}C_4X_1 \tag{7}$$

$$ET_2 = (PET - ET_1)\left(\frac{X_2}{X_2^0}\right)^{m3} \tag{8}$$

$$GW = C_2X_2 \tag{9}$$

in which X_1^0 is upper zone water capacity (millimeter), P is precipitation corrected with snow accumulation/snowmelt, SR is surface runoff, ET_1 is evapotranspiration from upper soil, INT is interflow, PC is percolation, X_2^0 is lower zone water capacity (millimeter), ET_2 is transpiration from lower soil, GW is groundwater flow, m_1 is runoff exponent, C_1 is interflow recession coefficient (per day), C_2 is coefficient in the percolation function, C_3 baseflow recession coefficient (per day), m_2 is exponent in the percolation function, m_3 is exponent in the function for transpiration from lower soil, and C_{FRG} is frozen ground coefficient.

Another parameter μ arises from baseflow, and is related to the fraction of groundwater flow that contributes to channel baseflow (BF),

$$BF = \left(\frac{1}{1+\mu}\right)GW + INT \tag{10}$$

A kinematic channel routing model is utilized to time distribute the channel inflows produced by the hydrologic component of 3R. A cascade of two conceptual reservoirs was used to simulate the water flow of a natural stream network. This model is based on the formulation originally proposed by *Mein et al.* [1974] and brought to a state-space form by *Georgakakos and Bras* [1982]. The channel routing model contains two parameters that define the relationship between the storage and the outflow of each of the conceptual reservoirs. We assumed that the reservoirs are linear. Therefore, the routing model requires the calibration of just one parameter (α). It is noted that the relationship implies a one-to-one correspondence between discharge and stage which is a characteristic of kinematic channel routing methods. The kinematic routing equations are given below,

$$\frac{dS_1}{dt} = (SR + BF) - \alpha S_1 \tag{11}$$

$$\frac{dS_2}{dt} = \alpha S_1 - \alpha S_2 \tag{12}$$

in which S is conceptual reservoir storage (millimeters), α is routing coefficient (per day), and dependence of states and fluxes on t is implied. Equations (11) and (12) were integrated numerically with an adaptive-stepsize, fourth-order Runge-Kutta procedure (maximum stepsize was 5 hours).

The parameters of the snow model were calibrated for the Upper Des Moines River basin by *Bae and Georgakakos* [1992] for a modified version of the Sacramento model and were assumed to be adequate for 3R. The coefficient C_{FRG} depends on temperature indices and snow model parameters [*Anderson and Neuman*, 1984]. Therefore, 3R requires the calibration of ten parameters with daily series of mean-areal precipitation, potential evapotranspiration [*Bae and Georgakakos*, 1992], minimum and maximum temperature and streamflow. The percolation exponent (m_2) and the lower soil transpiration exponent (m_3) were reported as 1.8 and 1.0, respectively, by *Bae and Georgakakos* [1994]. An automatic procedure to find the optimal set of the remaining eight parameter values was used. We applied the Downhill Simplex Method [*e.g., Press et al.*, 1986] for estimating both the soil accounting and routing model parameters. This method has been extensively used for calibrating conceptual hydrologic models [*e.g., Bae and Georgakakos*, 1994; *Duan et al.*, 1992;

Table 3. Ratio of Satellite and Rain Gauge Rainfall to the Threshold P_τ

Basin	P_τ=0.0, mm d^{-1}	P_τ=1.0, mm d^{-1}	P_τ=2.0, mm d^{-1}	P_τ=2.5, mm d^{-1}
Boone	0.80	0.73	0.71	0.69
West Fork	1.35	0.96	0.81	0.76
Des Moines	1.59	1.16	1.02	0.96

Table 4. Description and Optimal Parameter Sets for 3R Calibration with Mean-Areal Rain Gauge (RAI) and Satellite Rainfall (SAT)

Parameter	Description	Boone		West Fork		Des Moines	
		RAI	SAT	RAI	SAT	RAI	SAT
X_1^0, mm	Upper zone water capacity	119.0	127.3	195.2	212.2	118.1	168.9
X_2^0, mm	Lower zone water capacity	124.9	102.6	123.0	59.6	130.2	111.7
m_2	Runoff exponent	3.20	1.78	2.67	2.03	1.46	1.49
C_1, d^{-1}	Interflow recession coefficient	0.00070	0.00004	0.00060	0.00060	0.00100	0.00010
C_2	Coefficient in the percolation function	134.1	121.2	245.1	203.8	132.16	90.78
C_3, d^{-1}	Baseflow recession coefficient	0.0018	0.0004	0.0025	0.0013	0.0050	0.0044
μ	1/(1+m) Groundwater fraction that contributes to baseflow	1.99	1.51	3.26	0.00	4.03	3.04
α, d^{-1}	Coefficient of routing reservoirs	0.43	0.39	0.19	0.17	0.24	0.25
m_2	Exponent in the percolation function	1.8	1.8	1.8	1.8	1.8	1.8
m_3	Exponent in the function for transpiration from lower soil	1.0	1.0	1.0	1.0	1.0	1.0

Sorooshian et al., 1993]. The calibration procedure consists of running the model for an arbitrary set of parameters and comparing daily simulated outflows to the measured ones. Changes in parameter values are then effected to reduce an index to be minimized. Both the average residual and mean square error of daily predictions and observations are minimized by fine-tuning the parameter set. Table 4 shows the optimal parameter set for the three basins forced either with mean-areal rain gauge or satellite rainfall. Table 5 shows the corresponding daily streamflow statistics. The satellite rainfall forcing was simulated for the period May-September (with 60% of annual precipitation), whereas rain gauge forcing was used for the remaining months. The 3R calibration used 10 years of daily precipitation, potential evapotranspiration and streamflow for Boone (1979-1988), West Fork (1978-1987), and Des Moines (1979-1988).

There are important implications on using satellite rainfall forcing for calibrating the 3R parameters. Satellite rainfall estimates are characterized by a negative bias and a smaller variability than rain gauge mean-areal rainfall estimates. The satellite rainfall bias affects the parameters associated with the soil lower layers, by reducing the lower soil water capacity, percolation from upper to lower soil, baseflow, and groundwater replenishment. The smaller variability of satellite rainfall increases the upper soil capacity, which is one of the two parameters for runoff production.

The 3R model conserves streamflow volume and reproduces both high- and low-flow events (from daily to decadal scales), despite the negative bias in satellite rainfall. The cross correlation of simulated and observed streamflow for rain gauge data (ρ=0.88-0.90) was higher than the one for satellite rainfall (ρ=0.77-0.85). Both the estimated upper and lower soil water contents are characterized by interannual and seasonal variability, with the upper soil variation having larger amplitude than the lower soil. Figures 2 and 3 depict the 10-year estimates of pentad climatologies of streamflow and upper soil, obtained with rain gauge mean-areal precipitation and satellite rainfall forcing, for Boone (West Fork results, not shown, are similar to Boone) and Des Moines, respectively.

Figure 2a shows the pentad climatology of observed flows and the standard deviation of streamflow residuals (model-observed flow) for rain gauge model calibration and forcing, and satellite rainfall calibration and forcing. The model preserves the phase of the observed annual cycle of outflows for both rain gauge and satellite data. The amplitude of the first peak (March-April, pentads 12-24) is captured with both rain gauge and satellite-rainfall data, whereas the second peak (June-July, pentads 30-42) is underestimated with satellite rainfall. The largest streamflow simulation error with satellite data coincided with the period of heavy rains (June-July, pentads 30-42), which are underpredicted by the satellite estimation procedure. The streamflow errors with satellite rainfall remain larger than the errors with rain gauge forcing in autumn; since satellite rainfall is only imposed for May-September, these errors are related to the antecedent soil water conditions which were forced by satellite rainfall. Figure 2b shows the pentad climatology of upper soil water content in Boone for both rain gauge and satellite data. The climatological phase, amplitude (50 mm) and interannual variability of the upper soil water content was similar for both rain gauge and satellite rainfall.

The drainage area of Des Moines is 6 times larger than the Boone basin resulting in a more attenuated basin response to rainfall forcing, as shown by the smoother streamflow pentad

Table 5. Summary of the 10-Year Daily Flow

10-year	Boone			West Fork			Des Moines		
Climatology	OBS	RAI	SAT	OBS	RAI	SAT	OBS	RAI	SAT
Flow average	0.68	0.68	0.68	0.49	0.49	0.49	0.60	0.61	0.61
Flow standard deviation	1.15	1.15	0.89	0.73	0.67	0.59	0.78	0.77	0.72
Residual (mod-obs) average	-	0.00	0.00	-	0.00	0.00	-	0.01	0.01
Residual standard deviation	-	0.56	0.70	-	0.34	0.47	-	0.35	0.41
Cross correlation	-	0.88	0.80	-	0.88	0.77	-	0.90	0.85

Ten-year daily flow (in millimeters per day) statistics for the three basins, in which OBS: stream gauge flow, RAI: 3R flow predicted with rain gauge mean-areal precipitation, and SAT: 3R flow predicted with satellite rainfall.

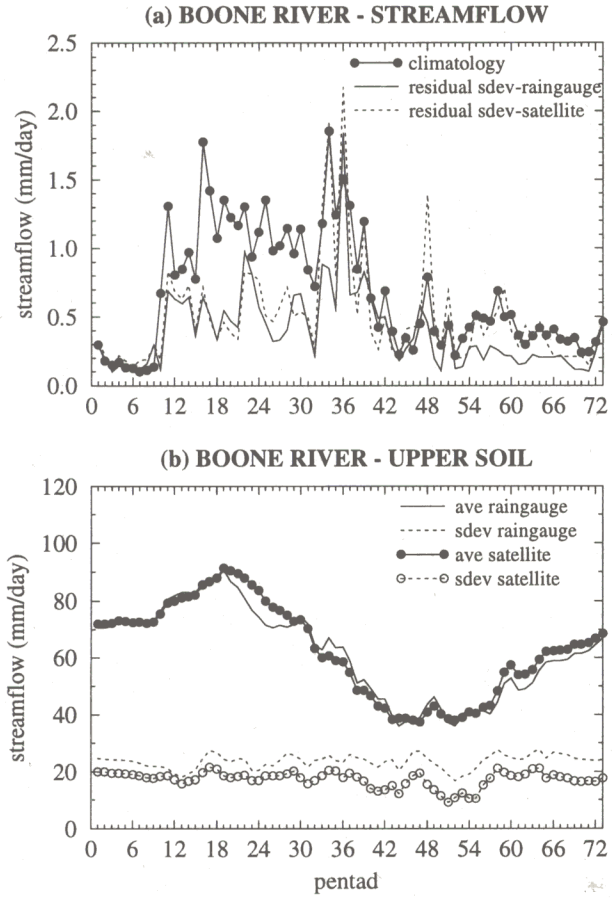

Figure 2. Streamflow prediction errors and soil water estimates for Boone. (a) Observed streamflow climatology and prediction errors. (b) Upper and lower soil climatology and interannual variability. Soil water and streamflow prediction errors were obtained for rain gauge-calibrated model forced with rain gauge mean-areal precipitation and satellite-calibrated model forced with satellite rainfall. Period with satellite forcing: pentads 24-56.

climatology of Figure 3a. The use of satellite rainfall data attenuates the streamflow peaks in midsummer (pentads 30-36) and early fall (pentads 48-54), corresponding to the spikes of the standard deviation of satellite rainfall residuals (model-observation). The climatological distributions of streamflow prediction errors with rain gauge and satellite data are similar, except for the aforementioned spikes in midsummer and early fall. The pentad climatology of upper soil water for Des Moines, depicted in Figure 3b, is characterized by similar phase and interannual variability for rain gauge and satellite rainfall. However, satellite rainfall yields larger amplitude (75 mm) than rain gauge data (50 mm).

In this investigation we have selected a perturbation analysis for quantifying the sensitivity of predicted streamflow to the model parameters. The distinguishing feature of rainfall runoff models is that a given parameter usually affects predicted runoff for more than one event, because the influence through time is transmitted by antecedent soil water conditions. The perturbation method consists in varying a specific parameter about its nominal value, while all the other parameters are kept constant, and tallying the associated error measure. The 3R flow simulation sensitivities to the prescribed parameters were similar for both rain gauge and satellite rainfall forcing. Sensitivities of predicted streamflow variability to the 10 model parameters indicated that the surface runoff exponent (m_1) and channel routing coefficient (α) are the main source of model simulation errors, whereas soil water capacity (upper and lower) and the parameters of the percolation function yield errors that are 50 - 20% of the m_1 and α errors. The model streamflow simulations vary weakly with changes in the interflow coefficient (C_1) and in the partitioning of groundwater flux into baseflow and groundwater replenishment (μ).

5. Streamflow Simulation

The sensitivity of the model to the mean-areal precipitation input focused on two issues: errors in forcing a rain gauge-calibrated model with satellite rainfall, and errors associated with the drainage basin scale. The former issue arises when models calibrated with historical rain gauge data are used in real-time prediction with satellite input when no automated rain gauge records are available. The latter issue is fundamental to the inference of soil water from remotely sensed data.

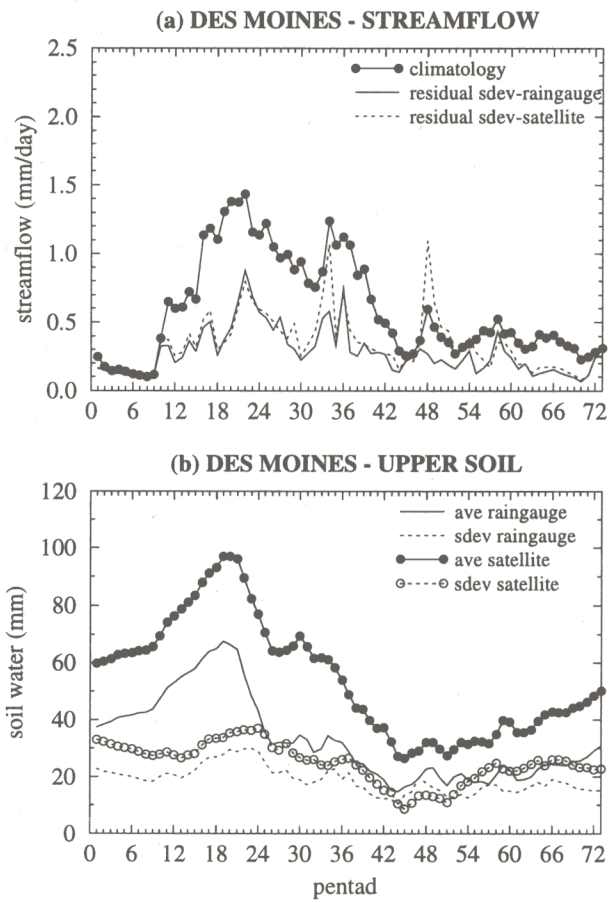

Figure 3. Streamflow prediction errors and soil water estimates for Des Moines. (a) Observed streamflow climatology and prediction errors. (b) Upper and lower soil climatology and interannual variability. Soil water and streamflow prediction errors were obtained for rain gauge-calibrated model forced with rain gauge mean-areal precipitation and satellite-calibrated model forced with satellite rainfall. Period with satellite forcing: pentads 24-56.

Table 6. Summary of the 10-Year Daily Flow

10-year	Boone			West Fork			Des Moines		
Climatology	RAI- RAI	RAI-SAT	SAT-SAT	RAI- RAI	RAI-SAT	SAT-SAT	RAI- RAI	RAI-SAT	SAT-SAT
Ratio of residual average and long-term flow average	0.00	-0.36	0.00	0.00	-0.39	0.00	0.02	-0.08	0.01
Ratio of residual and long term flow standard deviations	0.48	0.65	0.61	0.46	0.69	0.64	0.45	0.54	0.53
Daily cross correlation	0.88	0.76	0.80	0.88	0.73	0.77	0.90	0.84	0.85

Ten-year flow (in millimeters per day) statistics for the three basins, in which RAI-RAI: 3R calibrated and forced with rain gauge mean-areal precipitation; RAI-SAT: 3R calibrated with rain gauge data and forced with satellite rainfall; and SAT-SAT: 3R calibrated and forced with satellite rainfall.

Table 6 tallies the streamflow bias, variability, and cross correlation with observed flow for three conditions: (1) 3R calibrated and forced with rain gauge precipitation (RAI-RAI), (2) 3R calibrated with rain gauge data and forced with satellite rainfall (RAI-SAT), and (3) 3R calibrated and forced with satellite rainfall (SAT-SAT).

The model parameter calibration is designed to produce unbiased ensembles of simulated streamflow with minimum least-square variability. Therefore, the simulated streamflow bias is negligible for RAI-RAI and SAT-SAT. However, normalized streamflow error variability for SAT-SAT was 8-18% larger than for RAI-RAI. Forcing the rain gauge-calibrated model with satellite rainfall underestimates streamflow significantly. The 31% and 23% satellite rainfall underestimation yields a 36% and 39% decrease on simulated streamflow for Boone and West Fork, respectively; whereas the 4% negative bias in satellite rainfall causes a 8% streamflow underestimation for the larger Des Moines basin. The error (normalized standard deviation of residuals between simulated and observed streamflow) is the highest for the RAI-SAT case, exceeding 60% of the observed streamflow variability for Boone and West Fork.

The pentad climatologies of streamflow errors are shown in Figures 4 and 5, for Boone and Des Moines, respectively. The

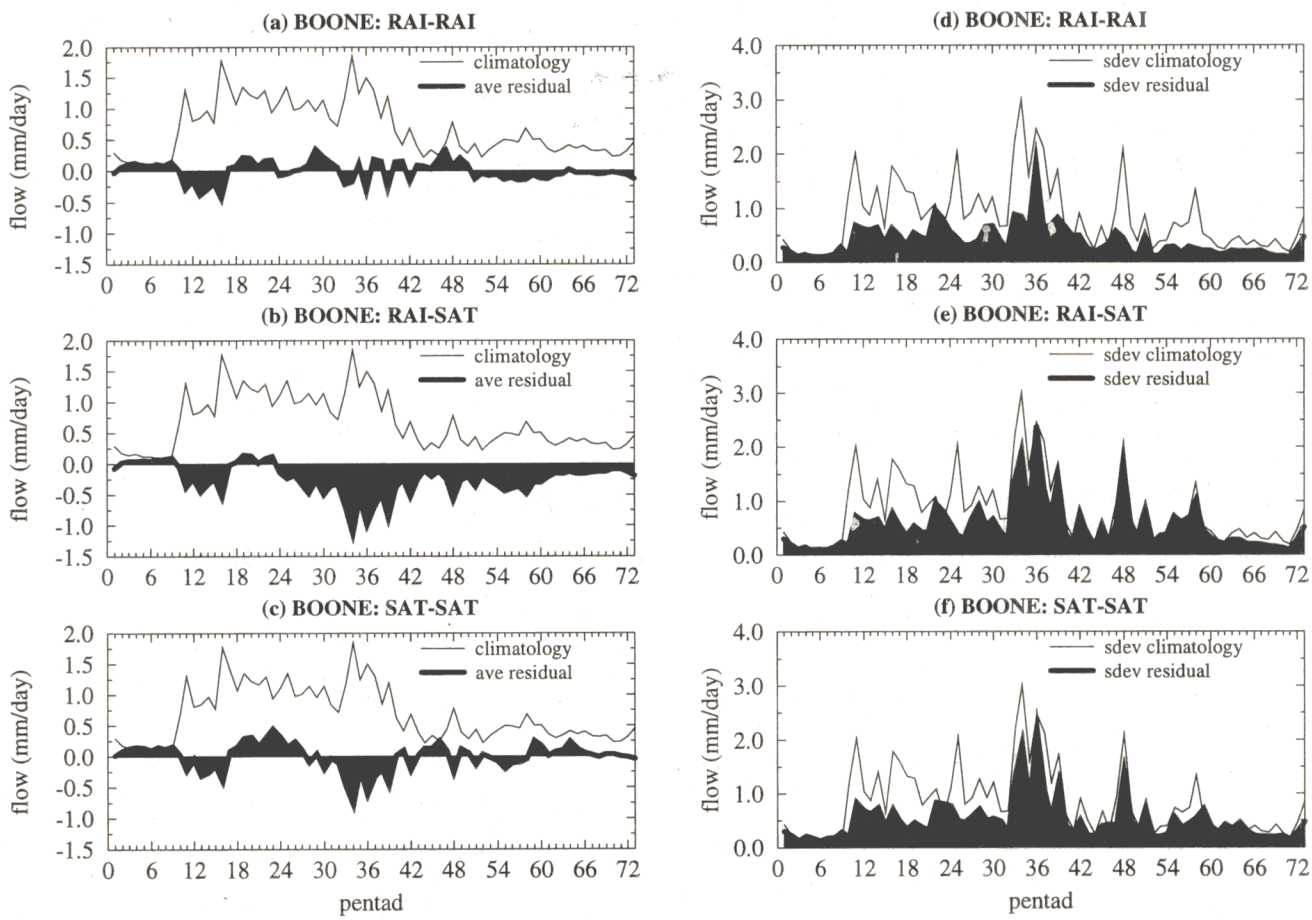

Figure 4. (a-c) Pentad climatologies of streamflow bias and (d-f) errors for Boone, in which RAI-RAI: 3R calibrated and forced with rain gauge mean-areal precipitation; RAI-SAT: 3R calibrated with rain gauge data and forced with satellite rainfall; and SAT-SAT: 3R calibrated and forced with satellite rainfall. Period with satellite forcing: pentads 24-56.

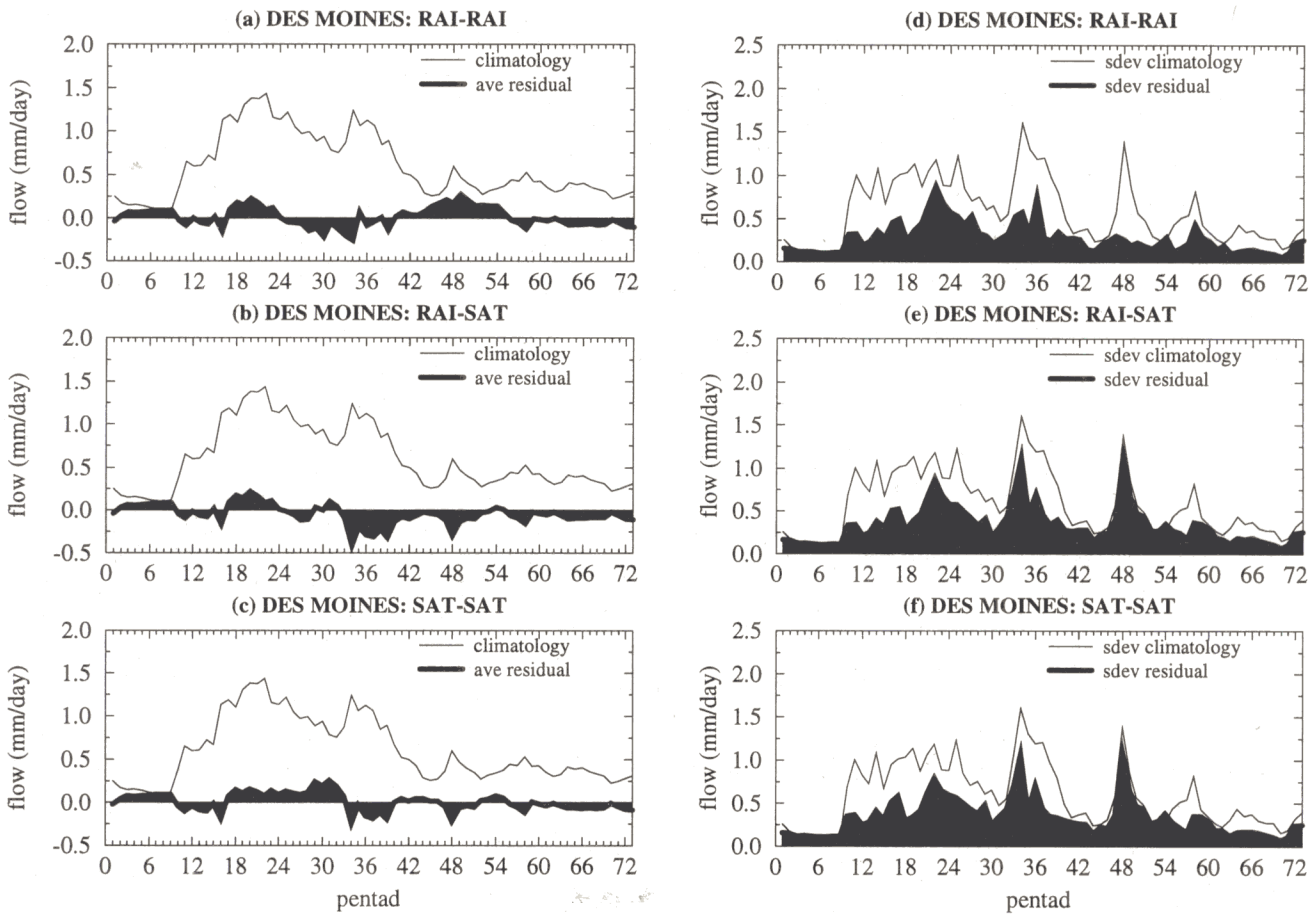

Figure 5. (a-c) Pentad climatologies of streamflow bias and (d-f) errors for Des Moines, in which RAI-RAI: 3R calibrated and forced with rain gauge mean-areal precipitation; RAI-SAT: 3R calibrated with rain gauge data and forced with satellite rainfall; and SAT-SAT: 3R calibrated and forced with satellite rainfall. Period with satellite forcing: pentads 24-56.

error distributions for Boone and West Fork are similar. Therefore, Boone's results are considered to be representative of smaller scales (~2,000-3,000 km^2), and Des Moines' results correspond to larger scales (~14,000 km^2), hereinafter. Figure 4a-4c depicts the bias of streamflow estimates for the different combinations of model parameters and precipitation input. Streamflow is underestimated during most of the year for RAI-SAT (Figure 4b), with the largest bias in midsummer, whereas the negative bias is substantially reduced when satellite input is given to a model calibrated with satellite rainfall. The streamflow error variability shown in Figure 4e-4f, indicates that prediction errors are of the same order magnitude of streamflow interannual variability during summer and fall for RAI-SAT and SAT-SAT.

Figure 5a-5c indicates that the Des Moines' modeled streamflow bias is of the same order of magnitude for the three combinations of model calibration and precipitation input, with satellite rainfall consistently underestimating streamflow in midsummer. The streamflow root-mean-square error is of the same order of magnitude as the streamflow interannual variability in mid summer and early fall (Figure 5e-5f) for the two models forced with satellite rainfall.

6. Soil Water Estimates and Scaling

Soil water is depth-integrated soil moisture averaged over a certain area. The depth of integration encompasses soil moisture available for evapotranspiration, surface runoff, and baseflow. Soil water behavior on scales of interest in this study remains largely unknown, since there are no direct measurements (the national programs for soil moisture measurement were reported by *Georgakakos and Baumer*, [1996]). *Huang et al.* [1996] estimated monthly soil water for all the 344 U.S. climate divisions using a water balance model with monthly precipitation and monthly mean temperature given as input. Model-estimated soil water for the Upper Des Moines River basin was discussed by *Georgakakos and Bae* [1994] based on 37-year series of daily rain gauge precipitation and evapotranspiration. It was reported that the range of the annual cycle of monthly averaged soil water for Boone, West Fork, and Des Moines ranged from 50 to 70 mm, and it was of the same magnitude as the interannual variability of monthly soil water. The lower and upper soil water were out-of-phase in early spring, when the upper soil volume peaks due to rain and snowmelt, and reduced percolation to the lower layers, suggesting an extended hydrologic response to frozen ground in winter [*Georgakakos et al.*, 1995a]. *Cayan and Georgakakos* [1995] investigated the spatial patterns and scales of monthly seasonal hydrologic-meteorologic anomalies associated with model-estimated soil water fluctuations for Boone, and suggested that basin average soil water extremes are meteorologically important to characterize the land-air connection on regional scales.

In this study, we reproduced the soil water features described by *Georgakakos and Bae* [1994] for the period of record 1949-1988, and expanded the analysis to identify the effect of satellite rainfall on soil water. Figures 6 and 7 show the pentad soil water climatology and standard deviation for Boone (smaller scale) and Des Moines (larger scale), respectively, for the model and forcing combinations RAI-RAI, RAI-SAT, and SAT-SAT. The climatological cycle of lower soil water is bimodal, with a first peak in early summer (pentad 30) and a second peak in early winter (pentads 66-72), and the phase does not change with satellite input. Soil water estimates varied significantly with respect to model calibration; that is, the amplitude of the soil water cycles was substantially attenuated when the satellite-calibrated model is forced with satellite rainfall, whereas the rain gauge calibrated model yielded almost identical upper and lower soil water cycles for either rain gauge or satellite rainfall forcing. Figures 6d-6f and 7d-7f indicate that the interannual variabilities of upper and lower soil water are of the same order of magnitude, except for Des Moines obtained with satellite-calibrated model forced by satellite rainfall. The interannual variability of pentad soil water is of the order of 20-30 mm, whereas the amplitude of the annual cycle ranges from 60-70 mm for upper and 30-50 mm for lower soil water pentads. It is noted that the frequency distribution of May-September upper soil water pentads for RAI-RAI favored dry conditions for Boone, whereas moderately wet conditions prevailed for SAT-SAT (not shown). The frequency distribution of RAI-SAT May-September upper soil water, with a total of 320 points, favored very dry conditions. Differences in the upper soil water frequency distribution for the three combinations of model and input for Des Moines (larger scale) were less significant than for Boone and West Fork (smaller scale). Therefore, model calibration and forcing may substantially affect the estimates of extreme soil water states.

The parametric scaling properties of estimated soil water for positive and negative anomalies were reported by *Georgakakos and Bae* [1994] for Boone. *Guetter and Georgakakos* [1996] proposed the nonparametric scale measure of spatiotemporal variability, ν_p, named Frequency Scaling Ratio. It is the probability that, over a given spatial scale, a certain soil water anomaly (positive or negative) will exceed in magnitude a threshold expressed in quantiles of the observed frequency distribution of anomalies. The behavior of ν_p computed from estimated soil water data may be compared to its expected behavior under purely random conditions, which provides the significance level for this analysis. The measure ν_p is given by the ratio

$$\nu_p = \frac{F_1(A \cap B)}{F_2(A \cup B)} \tag{13}$$

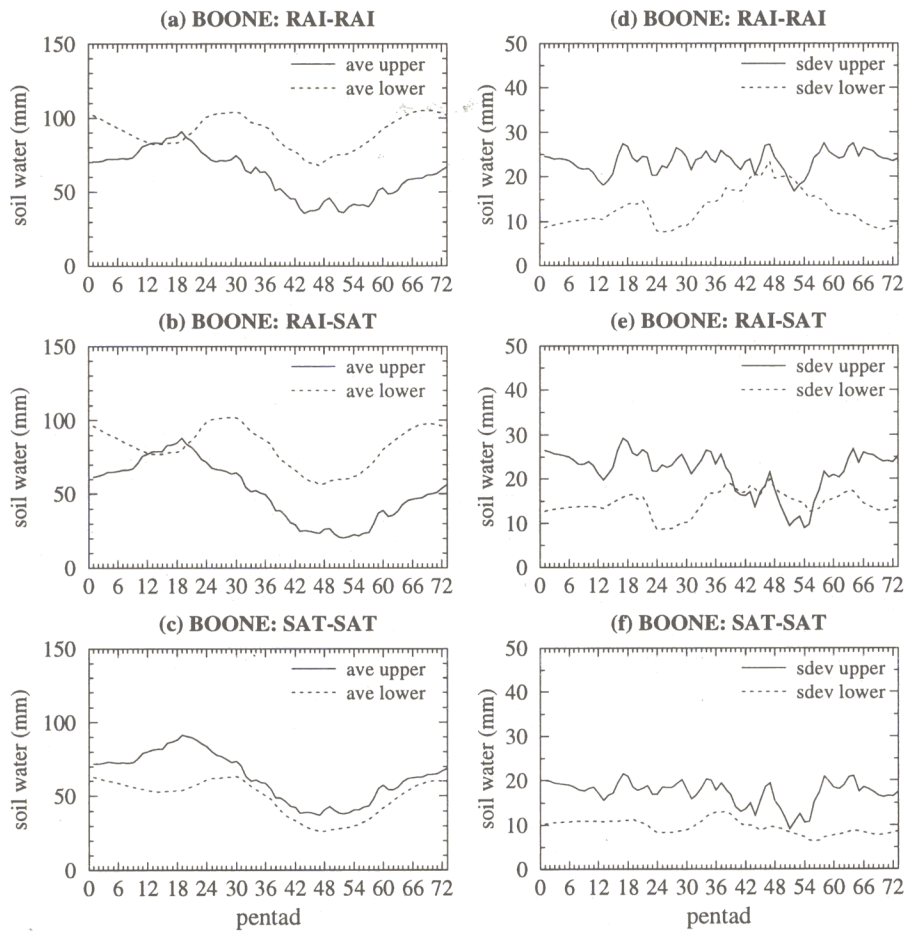

Figure 6. (a-c) Pentad climatologies of upper and lower soil water and (d-f) corresponding standard deviations for Boone, in which RAI-RAI: 3R calibrated and forced with rain gauge mean-areal precipitation; RAI-SAT: 3R calibrated with rain gauge data and forced with satellite rainfall; and SAT-SAT: 3R calibrated and forced with satellite rainfall. Period with satellite forcing: pentads 24-56.

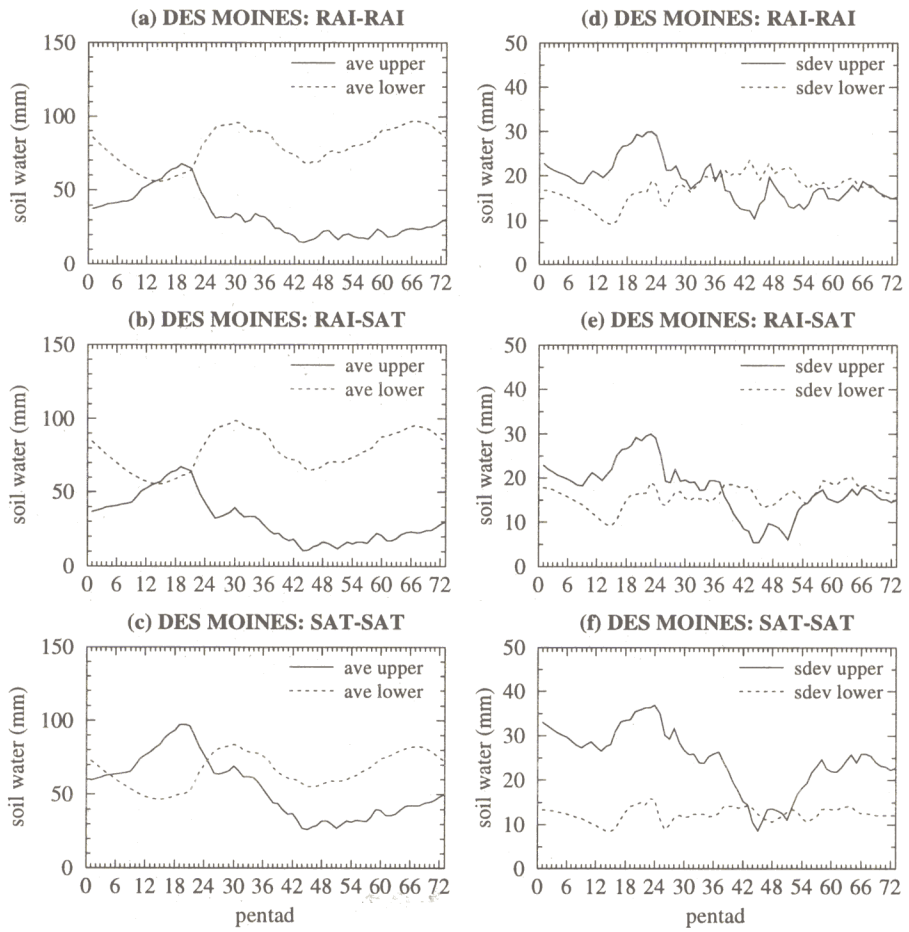

Figure 7. (a-c) Pentad climatologies of upper and lower soil water and (d-f) corresponding standard deviations for Des Moines, in which RAI-RAI: 3R calibrated and forced with rain gauge mean-areal precipitation; RAI-SAT: 3R calibrated with rain gauge data and forced with satellite rainfall; and SAT-SAT: 3R calibrated and forced with satellite rainfall. Period with satellite forcing: pentads 24-56.

with F_1 representing the number of time steps when the anomalies in both regions A and B exceed the set threshold q (in which q is a nonparametric anomaly, $0 \le q \le 1$), and F_2 representing the number of times that either A or B will exceed the threshold q. Following standard probabilistic nomenclature, the symbol "$\cap$" signifies "intersection" of events and the symbol "$\cup$" signifies "union" of events. Also, F_1 and F_2 may be interpreted as frequencies if they are normalized by the total number of time steps.

For two regions (an embedded and an embedding region) with independent random process $\nu_{p(q=0.5)}=0.33$ corresponds to pure chance and, for independent processes, the values of $\nu_{p(q>0.5)}$ decrease from that value [see *Guetter and Georgakakos*, 1996]. The condition $\nu_{p(q=0.5)}=0.33$ implies that the probability that positive (or negative) anomalies of any magnitude will occupy both regions by chance is 0.33. Greater probabilities than that imply higher frequency of occurrence of large anomalies that cover both regions.

Figure 8 depicts the scaling function ν_p, applied to upper soil water, for the pair of larger embedding and smaller embedded regions (Boone and Des Moines); Figure 8a shows the RAI-RAI case, whereas Figures 8b and 8c show the RAI-SAT and SAT-SAT combinations, respectively. The threshold (q') indicated in the plots is such that, for positive anomalies, $q=0.5+q'$, and for negative anomalies, $q=0.5-q'$. The threshold $q'=0$ corresponds to median soil water storage, whereas $q'=0.5$ corresponds to extreme wet (dry) conditions for positive (negative) anomalies. In the three plots we also show by dashed lines the 5% (lower) and 95% (upper) quantiles of the sampling error distribution. The bounds were obtained from Monte Carlo simulation using a lag-1 Markov model. Figure 8a-8c indicates that positive and negative anomalies scale similarly, within the $0.2<q<0.8$ range of soil water anomaly distribution. The probability of concurrent soil water conditions on larger and smaller scales varies between 0.6 and 0.8, in the $0.2<q<0.8$ anomaly range; whereas for 20% extreme quantiles, extreme positive anomalies occur with lower frequency than negative ones. This is likely due to the fact that extreme positive soil water anomalies are forced by smaller-scale intense precipitation events.

Upper soil water scaling for the RAI-SAT case (Figure 8b) was similar to the RAI-RAI (Figure 8a) case, with a discontinuity at the 20% extreme quantile of the distribution ($q'=0.3$). However, the scaling for SAT-SAT (Figure 8c) suggests stronger spatial association for positive and negative anomalies, with a discontinuity at the 10% extreme quantile of soil water distribution. The bias in the satellite rainfall synthetic series caused an increase in the upper soil capacity, which in turn increases the upper soil water autocorrelation, and the probability that soil water anomalies remain concurrently associated on large and small-scales.

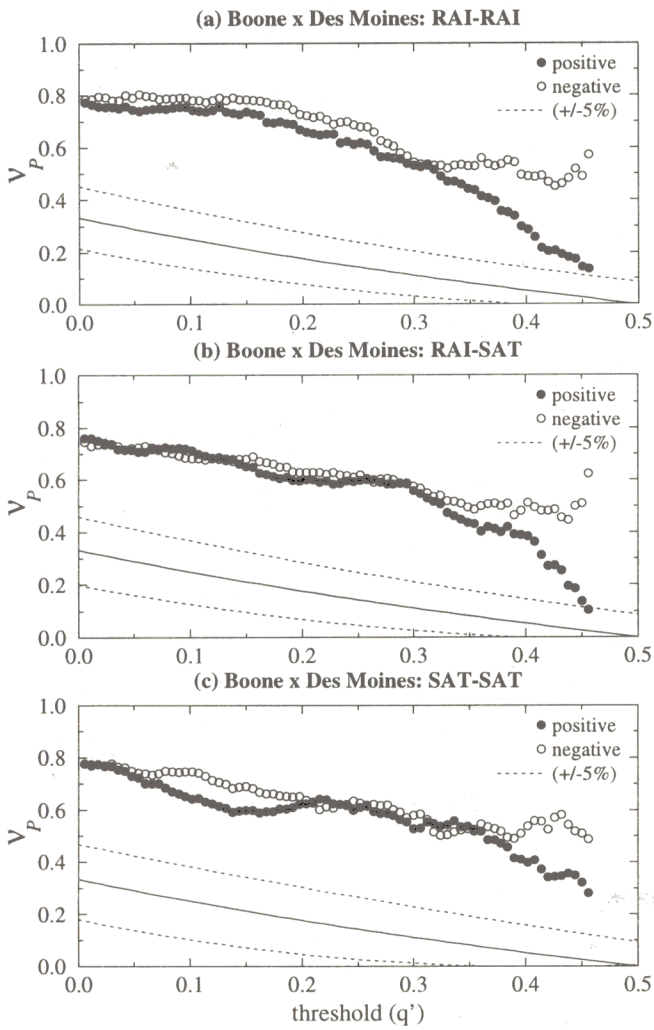

Figure 8. Frequency scaling ratio (FSR) as a function of soil water frequency threshold (q') for Boone and Des Moines. The threshold q' corresponds to (q-0.5) and (q+0.5) for negative and positive anomalies, respectively, where q is a certain quantile of the upper soil water distribution. (a) RAI-RAI: 3R calibrated and forced with rain gauge mean-areal precipitation; (b) RAI-SAT: 3R calibrated with rain gauge data and forced with satellite rainfall; and (c) SAT-SAT: 3R calibrated and forced with satellite rainfall. Period with satellite forcing: pentads 24-56.

7. Conclusions and Recommendations

A 180-day series of satellite rainfall estimates for a 70,000 km^2 area in the midwestern United States was used to identify the rain gauge satellite rainfall error structure, and build a 10-year synthetic series of daily satellite rainfall for climate studies. Satellite rainfall was estimated for the May-September period, in which satellite data was available. The constructed 10-year series of satellite rainfall used rain gauge mean-areal precipitation for the October-April period. Rain gauge and satellite rainfall were used to calibrate a hydrologic-hydraulic model (3R) that reliably simulates daily streamflow, and produces soil water estimates.

The principal conclusions of the study are as follows:

1. *Tsonis et al.* [this issue] derived satellite rainfall from a limited sample of infrared and visible data for the period May-September. We used these rainfall estimates to construct synthetic satellite rainfall for a 10-year period. The small sample size of satellite observations and scale effects cause the synthetic time series of satellite rainfall to underpredict the long-term climatology and interannual variability of rain gauge mean-areal precipitation. The synthetic satellite rainfall underpredicted mean-areal precipitation by 25 to 30% for Boone (2,000 km^2) and West Fork (3,500 km^2), and by 4% for Des Moines (14,000 km^2). The 10-year standard deviation of pentad reconstructed satellite rainfall varied from 60 to 65% (Boone and West Fork) to 80% (Des Moines) of the corresponding rain gauge data.

2. Flow simulation with a rainfall-runoff-routing hydrologic-hydraulic model forced with satellite rainfall is affected differently on different spatial scales. Using satellite data with rain gauge calibrated hydrologic models generates the following problems: (1) Simulated streamflow is biased, with flow being underpredicted by 36 to 39% for Boone and West Fork, and 8% for Des Moines; (2) the standard deviation of flow errors is 64 to 65% of observed flow interannual variability for the smaller basins, and is 54% for Des Moines; (3) the simulated streamflow error variance is of the same order of magnitude as the variance of streamflow due to interannual variance during summer and fall for the smaller basins, and during fall for the larger Des Moines basin.

3. There is no long-term streamflow bias for simulations with a satellite-calibrated model forced with satellite rainfall. However, the magnitude of the standard deviation of flow errors is of the same order of the ones obtained with rain gauge-calibrated models forced with satellite data (53 to 69% of streamflow interannual variability); the magnitude of streamflow errors varies with scale, with larger streamflow prediction errors found for smaller basins (Boone and West Fork).

4. Soil water climatology is substantially affected by the rainfall used for the hydrologic model calibration. The set of parameters obtained for the satellite-calibrated model yields smaller amplitude of the lower soil water cycle, whereas the amplitude of the upper cycle also varies with scale. The amplitude of upper soil water pentad climatology increased with satellite data (used in calibration and forcing) for larger basins (Des Moines).

5. The spatiotemporal scaling of soil water extremes is significantly affected by the rainfall forcing, indicating rainfall's important role for soil water, as suggested by *Cayan and Georgakakos* [1995] and *Guetter and Georgakakos* [1996]. The Frequency Scaling Ratio function, describing the spatiotemporal scaling of soil water anomalies, showed scale decreasing as the anomaly strength increases. The probability of concurrent normal soil water conditions (median) for larger and smaller basins is 80%, regardless whether rain gauge or satellite rainfall is used. For moderate soil water anomalies (within the middle 60% of the frequency distribution), the likelihood of occurrence of positive (wetter) and negative (drier) anomalies is similar. For extreme soil water anomalies (extreme 20% quantiles), the likelihood of large negative anomalies is higher than positive anomalies of the same magnitude. Spatiotemporal scaling of positive soil water anomalies is affected by satellite rainfall input. Scales of extreme positive anomalies (wetter) are likely to increase when satellite rainfall is used, approaching the scales of negative anomalies.

Perhaps the most important recommendation is to encourage the availability of a significant continuous record of

satellite data to support studies such the one reported herein. In such a way that possible biases and scale effects of satellite rainfall are resolved with actual satellite observations rather than with an error structure derived from a small sample. Until that time, studies such as the one reported herein are the only means of assessing the effects of satellite rainfall input to hydrologic models. Future research should address (1) the issue of reducing the impact of satellite errors in simulation and prediction by using streamflow measurements and state estimators to update soil water estimates in real time, and (2) coalescing satellite rainfall estimates with sparse rain gauge data to improve mean-areal rainfall estimates [*Green and Koren*, 1995].

Acknowledgments. This research was sponsored by NSF grants CMS-9496278 and BCS-9207943.

References

Adler, R.F., G.J. Huffman, and P.R. Keehn, Global tropical rain estimates from microwave-adjusted geosynchronous IR data, *Remote Sensing Rev.*, *11*, 125-152, 1994.

Anderson, E.A., and P.J. Neuman, Inclusion of frozen ground effects in a flood forecasting model, *Proceedings of the 5th Northern Research Basins Symposium*, The role of snow and ice in northern basin hydrology, Vierumaki, Finland, March 19-23, (5)1-(5)14, 1984.

Anderson, E.A., National Weather Service River Forecast System, Snow accumulation and ablation model, *NWS HYDRO-17, NOAA Tech. Memo.*, 1973.

Bae, D.-H., and K.P. Georgakakos, Climatic variability of soil water in the American Midwest, 1, Hydrologic modeling, *J. Hydrol.*, *162*, 355-377, 1994.

Bae, D.-H., and K.P. Georgakakos, Hydrologic modeling for flow forecasting and climate studies in large drainage basins, *IIHR Tech. Rep. 360*, 252 pp., Iowa Inst. of Hydraulic Res., Univ. of Iowa, Iowa City, 1992.

Cayan, D.R., and K.P. Georgakakos, Hydroclimatology of continental watersheds, 2, Spatial Analysis, *Water Resour. Res.*, *31*, 677-697, 1995.

Day, G.N., Extended streamflow forecasting using NWSRFS, *J. Water Resour. Plan. Manag.*, ASCE, *111*, 157-170, 1985.

Duan, Q., S. Sorooshian, and V. K. Gupta, Effective and efficient global optimization for conceptual rainfall-runoff models. *Water Resour. Res.*, *28*, 1015-1031, 1992.

Engman, T.E., Remote sensing, in *Handbook of Hydrology*, edited by D.R. Maidment, pp. 24.1-24.23, McGraw-Hill, New York, 1993.

Georgakakos, K.P., and O.W. Baumer, Measurement and utilization of on-site soil moisture data, *J. Hydrol.*, in press, 1996.

Georgakakos, K.P., D.-H. Bae, M.G. Mullusky, and A.P. Georgakakos, Hydrologic variability in midwestern drainage basins: diagnosis, prediction and control, in *Preparing for Global Change: A Midwestern Perspective*, edited by G.R. Carmichael, G.E. Folk and J.J. Schnoor, pp. 61-90, Academic, San Diego, Calif., 1995a.

Georgakakos, K.P., D.-H. Bae, and D.R. Cayan, Hydroclimatology of continental watersheds, 1, Temporal analysis, *Water Resour. Res.*, *31*, 655-675, 1995b.

Georgakakos, K.P., and D.-H. Bae, Climatic variability of soil water in the American Midwest, 2, Spatio-temporal analysis, *J. Hydrol.*, *162*, 379-390, 1994.

Georgakakos, K.P., and R. L. Bras, Real time, statistically linearized adaptive flood routing, *Water Resour. Res.*, *18*(3), 513-524, 1982.

Green, J.L., and V. Koren, Results using a simple weighting method to merge satellite and raingage data in the Blue Nile River basin for input into a Distributed Hydrological Model, *Conference on Hydrology*, 75th AMS Annual Meeting, Dallas, Texas, 173-177, 1995.

Guetter, A.K., and K.P. Georgakakos, Large-scale properties of simulated soil water variability, *J. Geophys. Res.*, *101*(D3), 7175-7183, 1996.

Huang, J., H.M. van den Dool, and K.P. Georgakakos, Analysis of model-calculated soil moisture over the U.S. (1931-93) and applications in long-range temperature forecasts, *J. Clim.*, in press, 1996.

Larson, L.W., and S. VanDemark, Mean-areal precipitation program (MAP), 1979, *National Weather Service River Forecast System (NWSRFS) user's manual*, Hydrol. Res. Lab., NWS, NOAA, Silver Spring, Md., 1979.

Mein, R.G., E.M. Laurenson, and T.A. McMahon, Simple nonlinear model for flood estimation, in *J. Hydraul. Div.*, Am. Soc. Civ. Eng., *100*(HY11), 1507-1518, 1974.

Negri, A.J., R.F. Adler, E.J. Nelkin, and G.F. Huffman, Regional rainfall climatologies derived from special sensor microwave imager (SSM/I) data, *Bull. Am. Meteorol. Soc.*, *75*, 1165-1182, 1994.

Peck, E. L., Catchment modeling and initial parameter estimation for the National Weather Service River Forecast System, Rep. *NWS HYDRO-31*, Natl. Oceanic and Atmos. Admin., Washington, D.C., 1976.

Press, W. H., B. P. Flannery, S. A. Teukolsky, and W. T. Vetterling, *Numerical Recipes.*, 818 pp., Cambridge University Press, New York, 1986.

Sorooshian, S., Q. Duan, and V. K. Gupta, Calibration of rainfall-runoff models: Application of global optimization to the Sacramento soil moisture accounting model, *Water Resour. Res*, *29*, 1185-1194, 1993.

Tsonis, A.A., G.N. Triantafyllou, and K.P. Georgakakos, Hydrological applications of satellite data, 1, Rainfall estimation, *J. Geophys. Res.*, this issue.

Wilheit, T., et al., Algorithms for the retrieval of rainfall from passive microwave measurements, *Remote Sensing Rev.*, *11*, 163-194, 1994.

K.P. Georgakakos and A.K. Guetter, Hydrologic Research Center, 12780 High Bluff Drive, Suite 260, San Diego, CA 92130. (e-mail: kpgeorga@hrc.ucsd.edu; akguette@hrc.ucsd.edu)

A.A. Tsonis, University of Wisconsin-Milwaukee, Department of Geosciences, P.O. Box 413, Lapham Hall, Milwaukee, Wisconsin, 53201. (e-mail: aatsonis@csd4.uwm.edu)

(Received November 1, 1995; revised May 9, 1996;
accepted May 15, 1996.)